Journal of Environmental Management 341 (2023) 118092

Contents lists available at ScienceDirect

Journal of Environmental Management

journal homepage: www.elsevier.com/locate/jenvman

Research article

The effects of biochar on soil organic matter pools are not influenced by climate change

Beatrice Giannetta [a], César Plaza [b], Michele Cassetta [c], Gino Mariotto [c], Iria Benavente-Ferraces [b], Juan Carlos García-Gil [b], Marco Panettieri [b], Claudio Zaccone [a,*]

[a] Department of Biotechnology, University of Verona, Strada Le Grazie 15, 37134, Verona, Italy
[b] Instituto de Ciencias Agrarias, Consejo Superior de Investigaciones Científicas, Serrano 115 bis, 28006, Madrid, Spain
[c] Department of Computer Sciences, University of Verona, Strada Le Grazie 15, 37134, Verona, Italy

ARTICLE INFO

Handling Editor: Dr. Lixiao Zhang

Keywords:
Particulate organic matter
Mineral-associated organic matter
Open top chambers
Fe EXAFS
Raman spectroscopy
Thermal analysis

ABSTRACT

The sustainability of Mediterranean croplands is threatened by climate warming and rainfall reduction. The use of biochar as an amendment represents a tool to store organic carbon (C) in soil. The vulnerability of soil organic C (SOC) to the joint effects of climate change and biochar application needs to be better understood by investigating its main pools. Here, we evaluated the effects of partial rain exclusion (~30%) and temperature increase (~2 °C), combined with biochar amendment, on the distribution of soil organic matter (SOM) into particulate organic matter (POM) and the mineral-associated organic matter (MAOM). A set of indices suggested an increase in thermal stability in response to biochar addition in both POM and MAOM fractions. The MAOM fraction, compared to the POM, was particularly enriched in labile substances. Data from micro-Raman spectroscopy suggested that the POM fraction contained biochar particles with a more ordered structure, whereas the structural order decreased in the MAOM fraction, especially after climate manipulation. Crystalline Fe oxides (hematite) and a mix of ferrihydrite and hematite were detected in the POM and in the MAOM fraction, respectively, of the unamended plots under climate manipulation, but not under ambient conditions. Conversely, in the amended soil, climate manipulation did not induce changes in Fe speciation. Our work underlines the importance of discretely taking into account responses of both MAOM and POM to better understand the mechanistic drivers of SOC storage and dynamics.

CRediT author statement

Beatrice Giannetta: Conceptualization; Investigation; Validation; Writing - original draft; Writing - review & editing. **César Plaza:** Conceptualization; Formal analysis; Funding acquisition; Supervision; Writing - review & editing. **Michele Cassetta:** Formal analysis; Investigation; Writing - review & editing. **Gino Mariotto:** Formal analysis; Investigation; Writing - review & editing. **Iria Benavente-Ferraces:** Investigation; Writing - review & editing. **Juan Carlos García-Gil:** Investigation; Writing - review & editing. **Marco Panettieri:** Investigation; Writing - review & editing. **Claudio Zaccone:** Conceptualization; Funding acquisition; Investigation; Validation; Resources; Supervision; Writing - review & editing.

1. Introduction

The Mediterranean region is experiencing the adverse effects of climate change through increasing temperatures and rainfall reduction (Perkins-Kirkpatrick and Gibson, 2017; Samaniego et al., 2018; Tramblay et al., 2020; IPCC, 2022). Both soil warming and drought may affect the microbial decomposition of soil organic carbon (SOC), and the multiple soil functions and services that SOC supports, such as food production, carbon (C) storage and climate regulation.

In this scenario, the application of biochar represents a strategy to store C in soil and counteract soil degradation in Mediterranean dryland environments (Lorenz and Lal, 2014; Plaza et al., 2018). The environmental and agronomic benefits of biochar, a highly aromatic C-rich material, have been extensively investigated (Sohi et al., 2010; Lehmann and Joseph, 2015; Grutzmacher et al., 2018; Sarauer et al., 2019) covering multiple aspects such as crop productivity, waste management

* Corresponding author.
E-mail address: claudio.zaccone@univr.it (C. Zaccone).

https://doi.org/10.1016/j.jenvman.2023.118092
Received 10 February 2023; Received in revised form 20 April 2023; Accepted 3 May 2023
Available online 9 May 2023
0301-4797/© 2023 Elsevier Ltd. All rights reserved.

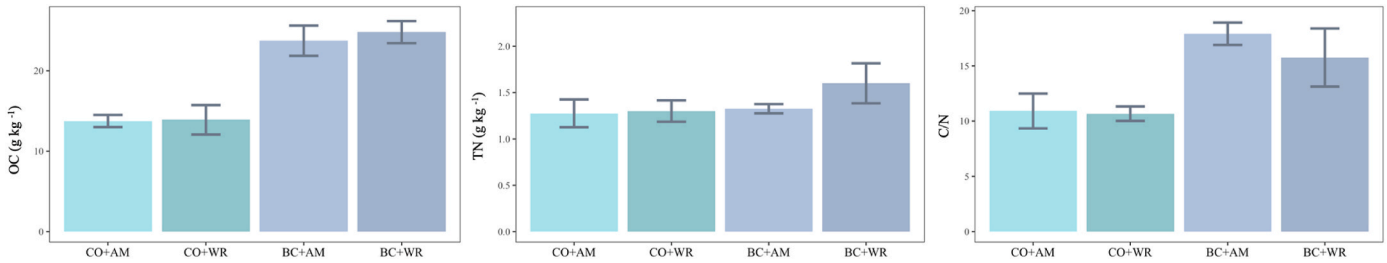

Fig. 1. Organic C (OC) and total N (TN) concentrations, and C/N ratio of unamended (CO) and biochar-amended (BC) soils under ambient (AM) and manipulated climate (WR, warming and rain exclusion) conditions. Error bars represent the standard deviation of the mean (n = 4).

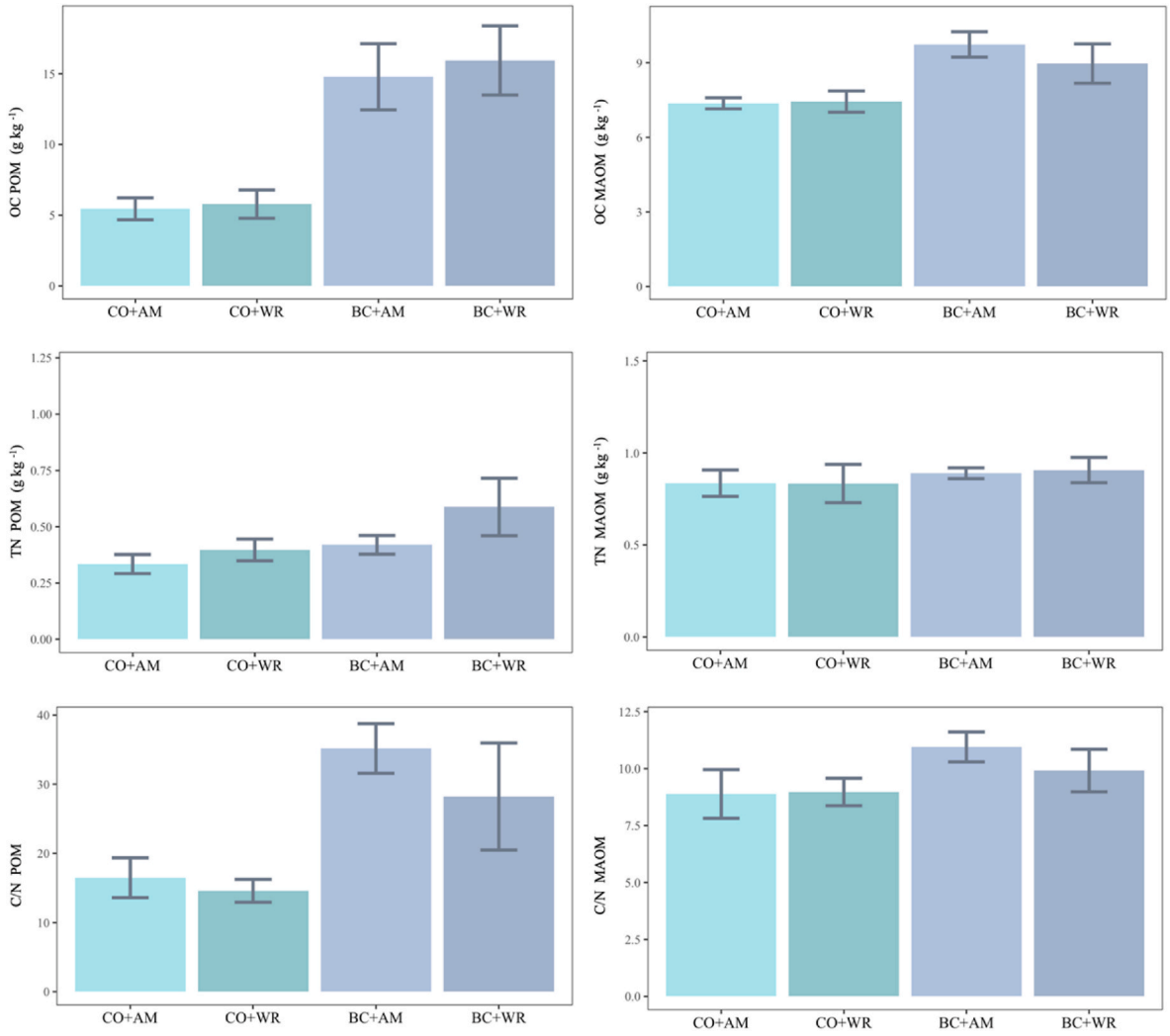

Fig. 2. Organic C (OC) and total N (TN) concentrations, and C/N ratio of particulate organic matter (POM) and mineral-associated organic matter (MAOM) fractions of unamended (CO) and biochar-amended (BC) soils under ambient (AM) and manipulated climate (WR, warming and rain exclusion) conditions. Error bars represent the standard deviation of the mean (n = 4).

and mitigation of global warming (Laird, 2008; Mathews, 2008; Atkinson et al., 2010; Woolf et al., 2010).

To comprehensively assess the agronomic and environmental benefits and risks of biochar, a better understanding of its interaction with native SOC is strongly needed (Hamer et al., 2004; Cross and Sohi, 2011; Wang et al., 2016a). Biochar may store native soil organic matter (SOM) within its porous network, limiting the accessibility to microbial decomposers and consequently reducing SOM turnover (Zimmerman et al., 2011; Yu et al., 2020; Bernard et al., 2022). Moreover, biochar may improve microbial proliferation and growth, providing a favourable habitat for microorganisms and acting as a retention hotspot of labile C, nitrogen (N), phosphorus and other micronutrients (Chan and Xu, 2009), and thus accelerating SOM decomposition.

Field experiments investigating biochar stability and its effects on native SOM are still scarce (Gurwick et al., 2013; Wang et al., 2016b). Furthermore, how changing climate conditions will affect SOM stabilization and destabilization in soils amended with biochar is mostly unknown (Poll et al., 2013; Bamminger et al., 2017; Grunwald et al., 2017). A more in-depth evaluation of strategies for C storage and of SOC vulnerability to climate change can be achieved by separating SOC into

Table 1
Analysis of variance for the effects of biochar (BC), climate manipulation (WR), and their interaction on organic C (OC), total N (TN), C/N ratio, and thermal indices ($WL_{400\text{-}550/250\text{-}350}$, TG-$T_{50}$, DSC-$T_{50}$) of whole soils, and particulate (POM) and mineral-associated organic matter (MAOM) fractions. *, **, and *** = significant at the 0.05, 0.01, and 0.001 levels. · = significant at the 0.1 level.

		OC Whole	TN Whole	C/N Whole	OC POM	TN POM	C/N POM	OC MAOM	TN MAOM	C/N MAOM	TG-T_{50} POM	TG-T_{50} MAOM	DSC-T_{50} POM	DSC-T_{50} MAOM	$WL_{400\text{-}550/250\text{-}350}$ POM	$WL_{400\text{-}550/250\text{-}350}$ MAOM
BC		***		***	***	·	***	***		**	***	**	*	***	***	
WR																
BC×WR			*			·								·		
CO + AM	**CO + WR**															
CO + AM	**BC + AM**	***		***	***		**	***		*	***	*		***	**	
CO + AM	**BC + WR**	***	**	**	***	***	*	**			**			***	**	
CO + WR	**BC + AM**	***		***	***		***	***		*	***	*	**	***	***	
CO + WR	**BC + WR**	***	**	**	***	**	**	*			***		*	***	**	
BC + AM	**BC + WR**		*			**								*		

functionally defined fractions: particulate (POM) and mineral-associated organic matter (MAOM) (Rocci et al., 2021). Being more protected from microbial degradation by soil minerals, MAOM is generally expected to be less prone to disturbance compared to POM.

Besides the virtually unknown effects of climate change on biochar performance in soil, the effects on SOC accrual into different fractions are contrasting and represent an additional uncertainty. We test whether climate change affects biochar behaviour in driving SOM accrual in both POM and MAOM fractions, and if changes dictated by decreasing precipitation alter iron (Fe) species involved in C storage. The objectives of this work were to investigate (a) the effect of biochar on the distribution of SOM in POM and MAOM pools, and (b) how climate change interacts with the effects of biochar and influences Fe speciation.

2. Material and methods

2.1. Experimental design

A field experiment was carried out in the experimental farm "La Poveda", Arganda del Rey (Spain). The experiment was established in 2012 with a randomized block design consisting in 4 blocks (Plaza et al., 2016; Moreno et al., 2022). The treatments used for this study included unamended control (CO) and amendment with biochar (BC) at a rate of 20 t ha^{-1} yr^{-1}. Biochar was broadcasted in fall 2012, 2013, 2014, 2016, and 2017 and immediately incorporated into the top soil (15 cm). Between October 2016 and February 2017, methacrylate rainfall shelters and open top chambers (OTCs; Suppl. Mat. Fig. S1) were placed to simulate a mean rainfall reduction of ~30% and a mean temperature increase of ~2 °C, respectively. Therefore, the experimental design consisted of two factors, *i.e.*, biochar application (unamended control, CO; and biochar application at 20 t ha^{-1} yr^{-1}, BC) and climate manipulation (ambient precipitation and temperature, AM; rain exclusion and warming, WR), and four treatments, *i.e.*, CO + AM, CO + WR, BC + AM, and BC + WR. More details about the study site, soil features and the experimental design are reported elsewhere (Plaza et al., 2016; Moreno et al., 2022) and summarized in the Supplementary Material.

In October 2021, soil samples were collected at 0–15 cm depth, air dried and 2-mm sieved prior to analyses.

2.2. Physical fractionation of SOM

Soils were fractionated by size following aggregate dispersion (Baldock et al., 2013; Cotrufo et al., 2019). Briefly, aliquots of 10.5 g of 2-mm sieved soil were stirred for 18 h in a 5 g L^{-1} sodium hexametaphosphate solution. Following dispersion, soil sample was sieved using a vibratory sieve shaker (AS 200, Retsch), thus resulting in a POM fraction (>53 μm) and a MAOM fraction (<53 μm). Each fraction was dried in the oven at 60 °C, weighed and ground using a zirconium ball mill (MM 400, Retsch).

2.3. Organic C and total N determination

The concentration of organic C and total N was determined in whole soil samples and SOM fractions by flash combustion using an elemental analyser (CHNS vario MACRO cube, Elementar, Germany). In particular, before organic C determination, both whole soil samples and SOM fractions underwent acid (HCl) fumigation in order to remove carbonates (Harris et al., 2001).

2.4. Thermal analysis

The thermal stability of SOM was assessed using a thermogravimetric analyzer coupled with simultaneous differential scanning calorimetry (TGA-DSC3+, Mettler Toledo, Switzerland). An aliquot of *ca.* 25 mg of sample was placed in an alumina crucible and heated from 30 to 700 °C at 10 °C min^{-1} under air using a flow rate of 100 mL min^{-1}.

2.5. Raman spectroscopy

Raman spectra were collected at room temperature using a micro-Raman spectrometer (Horiba Jobin-Yvon, model LabRam HR 800). The exciting radiation was provided by a He–Ne laser (λ_{exc} = 633 nm), whilst a narrow-band notch filter was used to cut the signal from the Rayleigh line to 200 cm^{-1}. A grating with 600 lines mm^{-1} was used to disperse the scattered radiation, which was then detected by a liquid N-cooled charge-coupled device detector (1024 × 256 pixels). A microscope coupled with a camera allowed the micro-analysis on selected micrometric-sized grains lying over a motorized XY stage. An 80 × LWD

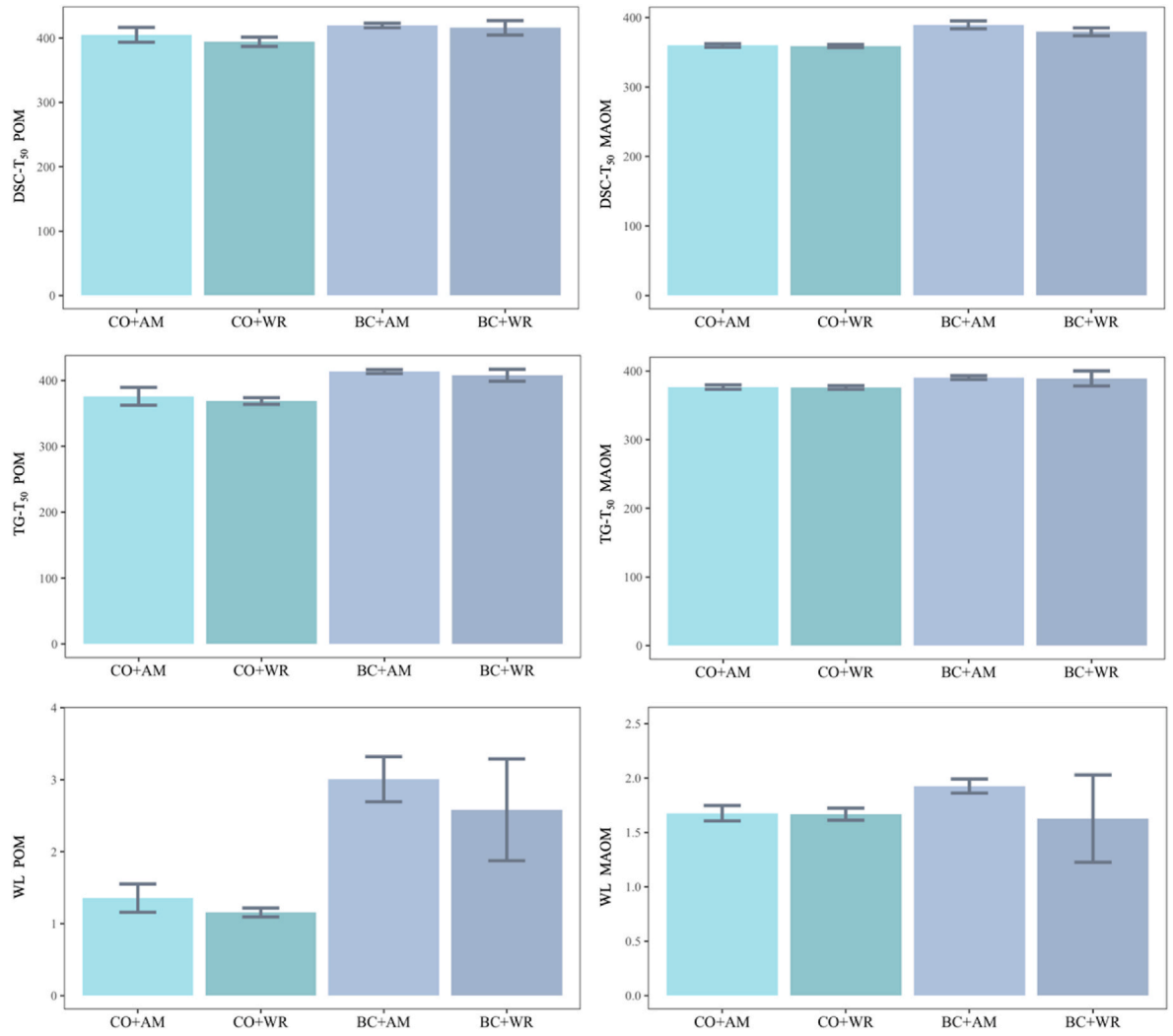

Fig. 3. Thermal indices of particulate organic metter (POM) and mineral-associated organic matter (MAOM) stability of unamended (CO) and biochar-amended (BC) soils, under ambient (AM) and manipulated climate (WR, warming and rain exclusion) conditions. DSC-T_{50} = temperature at which 50% of the energy is released in differential scanning calorimetry; TG-T_{50} = temperature at which half of mass is lost in thermogravimetry; WL = ratio of weight losses occurring between 400-550 and 250–350 °C. Error bars represent the standard deviation of the mean (n = 4).

objective, with numerical aperture of 0.75 and providing a laser-spot size (on the sample surface) of about 1.5 μm, was used to focus the laser beam on the surface of the selected grain. In order to collect artifact-free spectra (*i.e.*, phase transformation due to laser induced thermal treatment), every measure started with the lowest irradiation power possible. Afterwards, the laser power was increased step-wise up to a signal-to-noise ration maximized on the stable measured phase. This procedure was also accompanied by a visual inspection, allowing a further discrimination of eventual morphological changes originated by a laser-induced damages. Finally, a 4th degree polynomial anchored at 400, 900, 2200 and 3900 cm^{-1} was used to remove the luminescence background from the as-recorded spectra.

2.6. Fe extended X-ray absorption spectroscopy

X-ray absorption spectroscopic analysis of SOM fractions was carried out at the XAFS beamline at Elettra Sincrotrone (Trieste, Italy). Aliquots of *ca.* 15 mg of sample were powdered, pressed into pellets, sealed and mounted in a sample chamber. Fe extended X-ray absorption spectroscopy (EXAFS) spectra were collected in transmission mode using Si (111) monochromator, calibrated to the first-derivative maximum of the K-edge absorption spectrum of a metallic Fe foil, continuously monitored during measurements to detect small energy shifts. Linear combination fitting analysis was performed over a k-range of 2–10 $Å^{-1}$. EXAFS data processing and spectra generation were performed using the software Athena (Ravel and Newville, 2005). More details are reported elsewere (Giannetta et al., 2020, 2022).

2.7. Data analysis

The main and interaction effects of biochar amendment and climate manipulation were examined by analysis of variance (ANOVA) of linear mixed effects models, with an intercept random structure and block as the random factor. Degrees of freedom and F statistic were calculated by the Kenward-Roger method. Tukey tests at the 0.05 level were used for pairwise comparisons of marginal means. All data analyses were performed using R version 4.1.1 (R Core Team, 2021).

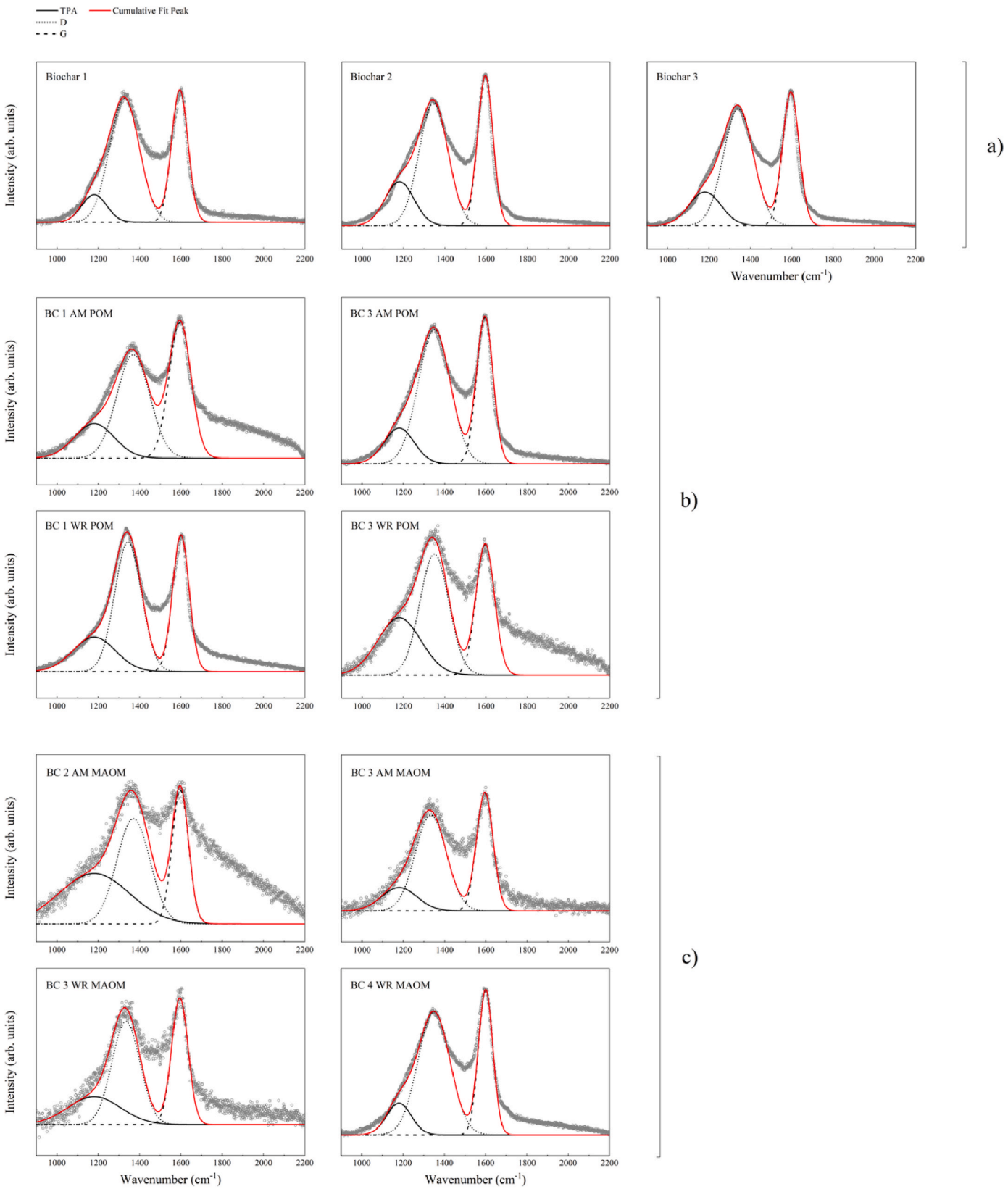

Fig. 4. Peak deconvolution of the Raman spectra of biochar (a), POM fractions (b) and MAOM fractions (c), under ambient (AM) and manipulated climate (WR, warming and rain exclusion) conditions. Spectra of samples having different I(D)/I(G) ratios are displayed.

3. Results and discussion

3.1. Organic C and total N distribution in SOM fractions

Biochar increased the content of SOC and those of its particulate and mineral-associated fractions (Figs. 1 and 2, Table 1), confirming its potential as an efficient strategy for C storage (Liu et al., 2016; Plaza et al., 2016; Yousaf et al., 2017). In contrast, the effect of climate manipulation and its interaction with biochar application were not significant (Table 1). Investigating soil samples collected in 2018 (*i.e.*, 3 years earlier) from the same experiment, Moreno et al. (2022) also found that only biochar affected SOC contents and ascribed the absence of climate effects to the short duration of the climate manipulation.

Total soil N was affected by neither biochar nor climate manipulation; however, an interaction between biochar and climate manipulation on the N content in the bulk soil (Fig. 1, Table 1) was detected. This effect may be attributed to a warming-induced shift from cellulolytic to ligninolytic enzymes activities and a shift in the composition of active fungal communities and litter chemistry (Morrison et al., 2019), that can result in a relative increase in N content. As a consequence of the increases in SOC, C/N ratios of POM and MAOM fractions were significantly higher in biochar amended soils than in unamended soils (Figs. 1 and 2; Table 1).

Altogether, biochar amendment increased organic C content both in the POM and in the MAOM fractions, whereas warming and rain exclusion, and their interaction with biochar, did not play a significant role. In detail, biochar amendment mainly affected organic C storage in the POM fraction. As a consequence, the MAOM/POM ratio was lower in the amended soil compared to the unamended one. Field experiments with climate manipulation simulating altered precipitation and warming, including biochar application, are scarce and often provide contrasting results (Sardans et al., 2008; Poll et al., 2013). Grunwald et al. (2017) reported that an increase of soil temperature of 2.5 °C had no effects on the organic C accrual in aggregate-size or density fractions and that the short-term rising soil temperatures had a minor effect on both the decomposition and distribution of SOM into different pools. Lugato et al. (2021) underlined that, especially in croplands, high organic C loss could occur, mainly in the MAOM, from the top 20 cm of mineral soils in the European Union between 2015 and 2080. Although the MAOM fraction is largely less prone to decomposition than POM, it may respond to variations in plant inputs and microbial activity; this is particularly true in soils where the MAOM represents the dominant form of organic C. Thus, the MAOM is generally less accessible, but not fully inaccessible. Therefore, a stabilization gradient concept should be considered, rather than parametrizing SOM as stabilized or not in MAOM.

3.2. Thermal stability of SOM pools

The first step of weight loss (WL) in thermogravimetric curves, occurring in the temperature range 250–350 °C, is ascribed to easily oxidizable compounds (*e.g.*, cellulose, hemicellulose) and aliphatic structures, while the second, recorded in the range 350–550 °C, to the degradation of more recalcitrant structures (*e.g.*, lignin and non-hydrolyzable compounds) (Schnitzer and Hoffman, 1966; Lopez-Capel et al., 2005; Plante et al., 2009).

The stability and recalcitrance of SOM can be described using several thermal proxies, including ratios between WL within defined temperature ranges, the temperature at which 50% of the SOM mass is lost (TG-T_{50}) and that at which 50% of the energy is released (DSC-T_{50}) (*e.g.*, Rovira and Vallejo, 2000; Lopez-Capel et al., 2005; Plante et al., 2009; Giannetta et al., 2022). The set of thermal indices used here ($WL_{400\text{-}550/250\text{-}350}$, TG-$T_{50}$, DSC-$T_{50}$) suggested a general increase in thermal stability in response to biochar addition in both fractions; on the opposite, warming and rain exclusion did not play a significant role (Fig. 3; Table 1). In detail, significantly greater DSC-T_{50} and TG-T_{50} were found for the POM and MAOM fractions in biochar-amended soils compared to the unamended soils (Fig. 3), while the ratio between WL in the range 400–550 and 250–350 °C ($WL_{400\text{-}550/250\text{-}350}$) was higher (2–3 ×) only for the POM fraction (Fig. 3). In fact, being biochar enriched in stable C compounds, the labile fraction was rapidly depleted and the mineralization of aromatic fractions usually slow, thus resulting in a quite high thermal stability of molecular compounds (Kuzyakov et al., 2014; Wang et al., 2016b). Climate manipulation seemed to not affect thermal stability of the SOM fractions, although a slight (but non significant) interaction between biochar application and warming was observed for the DSC-T_{50} of the MAOM fraction (Fig. 3; Table 1). The high standard deviations found exclusively for the BC + WR treatment may suggest the occurrence of more heterogeneous molecules possibly promoted by the warming in the short-term. To evaluate the effect on the long-term, follow-up samplings are needed.

3.3. Order/disorder in SOM pools from biochar amended soils

The Raman spectrum of a carbonaceous material shows two main peaks, that are the G ("graphitic")-peak (E_{2g}-symmetry) around 1580 cm^{-1} and the D ("defect")-peak around 1350 cm^{-1} (A_{1g}-symmetry). The G peak can be attributed to the bond stretching of all pairs of sp^2-bonded C atoms in both chains and rings, whereas the D peak is generally associated to the breathing mode of sp^2-bonded C atoms in hexagonal aromatic rings (Ferrari and Robertson, 2000, 2004). For amorphous C, the development of the D peak is an indicator of structural order (Ferrari and Robertson, 2000). Therefore, more prominent G and D peaks may suggest the decomposition and mineralization of more labile, unordered carbonaceous material and, consequently, a relative enrichment of hexagonal aromatic rings and a greater ordering of the biochar structure.

To acquire detailed information on the micro-Raman spectra, a 3-band deconvolution model (*i.e.,* Gaussian) was used; the curve fitting was carried out using the Origin® software. The fitting of the D and G bands was voluntarily released while only the position of the trans-polyacetilene (TPA)-like structure band was fixed at 1180 cm^{-1}, providing a better fitting profile on the shoulder to the left the D band (Ferrari and Robertson, 2001; Osipov et al., 2011; Bogdanov et al., 2014). The peak deconvolutions are illustrated in Fig. 4. The degree of structural order of a sample is expressed by the I(D)/I(G) ratio, *i.e.*, the ratio between the relative intensity of the D band *vs.* the G one. This relative intensity is directly proportional to the order of the nano-structure in carbonaceous substances with crystallite size <2 nm (Ferrari and Robertson, 2000) (*e.g.,* biochar). Thus, higher ordered biochar is supposed to be more recalcitrant. In amorphous C, the development of a D peak indicates ordering, exactly opposite from the case of graphite (Ferrari and Robertson, 2000). The Raman microspectroscopic analysis shows high I(D)/I(G) ratios in the POM fraction, indicating a quite high structural order. However, this fraction is highly heterogeneous, having an I(D)/I(G) ratio ranging from 1.35 ± 0.44 to 1.88 ± 0.32 in the BC + AM POM, with an average value of 1.65 ± 0.39 that does not differ from the average I(D)/I(G) ratio of the POM fraction after warming (BC + WR) (Table 2). In the MAOM fraction under ambient conditions the average I(D)/I(G) ratio ranges from 1.33 ± 0.09 to 1.82 ± 0.32, whereas in the MAOM after warming from 1.11 ± 0.05 and 1.63 ± 0.52 (Table 2). Thus, in the MAOM fraction this ratio tends to generally decrease after warming, thus confirming thermal data. This could be due

Table 2
Raman parameters calculated from the biochar-amended (BC, from 1 to 4) particulate (POM) and mineral-associated organic matter (MAOM) fractions under ambient conditions (AM) and rain exclusion and warming (WR). I(D) = intensity of the D band; I(G) = intensity of the G band; G-D = distance between D and G bands.

	ID/IG		G-D	
	Average	Std. dev.	Average	Std. dev.
BC1 AM POM	1.35	0.44	238.02	7.10
BC1 WR POM	1.43	0.21	239.13	3.76
BC1 AM MAOM	1.33	0.09	226.92	1.29
BC1 WR MAOM	1.11	0.05	232.46	4.29
BC2 AM POM	1.78	0.31	238.04	3.75
BC2 WR POM	1.61	0.30	235.10	6.77
BC2 AM MAOM	1.41	0.47	238.08	4.25
BC2 WR MAOM	1.63	0.52	238.29	4.61
BC3 AM POM	1.88	0.32	235.45	4.71
BC3 WR POM	1.93	0.18	234.78	8.64
BC3 AM MAOM	1.72	0.29	232.32	8.90
BC3 WR MAOM	1.48	0.40	232.25	8.46
BC4 AM POM	1.58	0.48	234.36	9.37
BC4 WR POM	1.62	0.12	235.72	6.84
BC4 AM MAOM	1.82	0.24	241.23	5.48
BC4 WR MAOM	1.51	0.39	237.55	1.84
Biochar	2.03	0.19	237.90	2.48

to an increase of the microbial activity, induced by both biochar amendment and warming, resulting in the production of randomly oriented organic molecules. Therefore, micro-Raman analysis confirms a different structural order of the graphitic-like structures in POM and MAOM fractions, and their evolution with warming.

3.4. Changes of Fe species due to warming and biochar amendment

Linear combination fitting allowed the identification of the major Fe species (n = 4) characterizing the fractions composition (Table 3). Fe EXAFS data fitting indicated that the Fe species of POM and MAOM are different, mainly in terms of Fe oxides composition. The POM fraction of the unamended soil was mainly characterized by chlorite and illite (sum *ca.* 60%), ferrihydrite (14%) and Fe(III)-SOM (28%). In the MAOM fraction, ferrihydrite represents the most important part of the fitting (more than 2 × higher than in POM), thus confirming data reported in Giannetta et al. (2020). Besides ferrihydrite, the formation of more crystalline Fe phases like hematite occurred after climate manipulation in both POM and MAOM. In the MAOM fraction, ferrihydrite was still the main Fe oxide, followed by hematite. In the amended soil, climate manipulation did not affect Fe speciation, whereas significant differences were found between the POM and MAOM fractions. In the amended soils under ambient conditions, both illite and chlorite occurred in the POM fraction; the remaining Fe phases mainly consisted of Fe(III)-SOM (17%) and hematite.

Biochar amendment decreased Fe(III)-SOM content in the POM fraction, compared to the unamended soil. In the MAOM fraction, besides hematite, also ferrihydrite occurred (*ca.* 20%), and the contribution from Fe(III)-SOM increased up to 27%. A similar trend was evident in both POM and MAOM from the BC + WR treatment. In detail, after climate manipulation, ferrihydrite was found in the MAOM fraction (27%), and Fe(III)-SOM increased in the MAOM (29%) compared to the POM (19%) fraction, whereas the Fe(III)-SOM contents in both fractions were not different in the unamended soil.

4. Conclusions

We provide evidence that SOM accrual in different fractions is affected by the application of biochar, but not by climate manipulation, and that climate manipulation does not interact significantly with biochar effects on SOC content and those of its fractions. Similarly, SOM thermal stability is affected by biochar but not by the interaction of biochar and climate manipulation. Raman data indicate that the POM fraction contains biochar particles with a more ordered structure, whereas in the MAOM fraction the structural order seems to decrease, especially after climate manipulation. Hovewer, further studies are still needed to evaluate the long-term effect of climate manipulation on the structural order and MAOM vulnerability. In the amended soil, climate manipulation does not induce changes in Fe speciation, whereas the main difference occurs between the POM and the MAOM fraction. Longer-term and seasonal monitoring experiments are highly needed to assess the evolution of SOM fractions under a climate change scenario and their interaction with the application of biochar, especially in Mediterranean semiarid agroecosystems.

Declaration of competing interest

The authors declare that they have no known competing financial interests or personal relationships that could have appeared to influence the work reported in this paper.

Data availability

No data was used for the research described in the article.

Table 3
Four component linear combination fitting performed on the k^3-weighted Fe K-edge EXAFS data of particulate organic matter (POM) and mineral-associated organic matter (MAOM) pools from agricultural soils under different management (unamended, CO; biochar amendment, BC) and climate manipulation (AM, ambient conditions; WR, rain exclusion and warming). Results are expressed as percentage of the fitting components corresponding to experimental spectra of model compounds.

	Component 1	%	Component 2	%	Component 3	%	Component 4	%	Sum
CO + AM POM	Chlorite	6	Illite	53	Ferrihydrite	14	Fe(III)-SOM	28	100
CO + AM MAOM	Chlorite	24	Illite	14	Ferrihydrite	33	Fe(III)-SOM	29	100
CO + WR POM	Chlorite	19	Illite	55	Hematite	6	Fe(III)-SOM	20	100
CO + WR MAOM	Illite	36	Ferrihydrite	29	Hematite	8	Fe(III)-SOM	28	100
BC + AM POM	Chlorite	16	Illite	57	Hematite	9	Fe(III)-SOM	17	100
BC + AM MAOM	Illite	43	Ferrihydrite	22	Hematite	7	Fe(III)-SOM	28	100
BC + WR POM	Chlorite	21	Illite	46	Hematite	14	Fe(III)-SOM	19	100
BC + WR MAOM	Illite	36	Ferrihydrite	27	Hematite	8	Fe(III)-SOM	29	100

Acknowledgements

This work has been supported by the Seal of Excellence programme, CLISOMAP project (ref. B37G22000790006). This research has also received funding from the European Union Horizon 2020 Research and Innovation Programme under Grant Agreement No. 101000224 (TUdi project). The authors finally acknowledge support from the Spanish Ministry of Science and Innovation (ref. TED 2021-132342B–I00).

Appendix A. Supplementary data

Supplementary data to this article can be found online at https://doi.org/10.1016/j.jenvman.2023.118092.

References

Atkinson, C.J., Fitzgerald, J.D., Hipps, N.A., 2010. Potential mechanisms for achieving agricultural benefits from biochar application to temperate soils: a review. Plant Soil 337, 1–18.

Baldock, J.A., Sanderman, J., Macdonald, L.M., Puccini, A., Hawke, B., Szarvas, S., McGowan, J., 2013. Quantifying the allocation of soil organic carbon to biologically significant fractions. Soil Res. 51, 561–576.

Bamminger, C., Poll, C., Marhan, S., 2017. Offsetting global warming-induced elevated greenhouse gas emissions from an arable soil by biochar application. Global Change Biol. 24, e318–e334.

Bernard, L., Basile-Doelsch, I., Derrien, D., Fanin, N., Fontaine, S., Guenet, B., Karimi, B., Marsden, C., Pierre-Alain Maron, P.-A., 2022. Advancing the mechanistic understanding of the priming effect on soil organic matter mineralization. Funct. Ecol. 36, 1355–1377.

Bogdanov, K., Fedorov, A., Osipov, V., Enoki, T., Takai, K., Hayashi, T., Ermakov, V., Moshkaev, S., Baranov, A., 2014. Annealing-induced structural changes of carbon onions: high-resolution transmission electron microscopy and Raman studies. Carbon 73, 78–86.

Chan, K.Y., Xu, Z., 2009. Biochar: nutrient properties and their enhancement. In: Lehmann, J., Joseph, S. (Eds.), Biochar for Environmental Management. Earthscan, London, U.K., pp. 67–84.

Cotrufo, M.F., Ranalli, M.G., Haddix, M.L., Six, J., Lugato, E., 2019. Soil carbon storage informed by particulate and mineral-associated organic matter. Nat. Geosci. 12, 989–994.

Cross, A., Sohi, S.P., 2011. The priming potential of biochar products in relation to labile carbon contents and soil organic matter status. Soil Biol. Biochem. 43, 2127–2134.

Ferrari, A.C., Robertson, J., 2000. Interpretation of Raman spectra of disordered and amorphous carbon. Phys. Rev. B 61, 14095.

Ferrari, A.C., Robertson, J., 2001. Origin of the 1150 cm^{-1} Raman mode in nanocrystalline diamond. Phys. Rev. B 63, 121405.

Ferrari, A.C., Robertson, J., 2004. Raman spectroscopy of amorphous, nanostructured, diamond-like carbon, and nanodiamond. Phil. Trans. Roy. Soc. Lond. 362, 2477–2512.

Giannetta, B., Plaza, C., Siebecker, M.G., Aquilanti, G., Vischetti, C., Plaisier, J.R., Juanco, M., Sparks, D.L., Zaccone, C., 2020. Iron speciation in organic matter fractions isolated from soils amended with biochar and organic fertilizers. Environ. Sci. Technol. 54, 5093–5101.

Giannetta, B., Plaza, C., Thompson, A., Plante, A.F., Zaccone, C., 2022. Iron speciation in soil size fractions under different land uses. Geoderma 418, 115842.

Grunwald, D., Kaiser, M., Junker, S., Marhan, S., Piepho, H.-P., Poll, C., Bamminger, C., Ludwig, B., 2017. Influence of elevated soil temperature and biochar application on organic matter associated with aggregate-size and density fractions in an arable soil. Agric. Ecosyst. Environ. 241, 79–87.

Grutzmacher, P., Puga, A.P., Bibar, M.P.S., Coscione, A.R., Packer, A.P., de Andrade, C. A., 2018. Carbon stability and mitigation of fertilizer induced N_2O emissions in soil amended with biochar. Sci. Total Environ. 625, 1459–1466.

Gurwick, N.P., Moore, L.A., Kelly, C., Elias, P., Sun, Q., 2013. A systematic review of biochar research, with a focus on its stability in situ and its promise as a climate mitigation strategy. PLoS One 8, e75932.

Hamer, U., Marschner, B., Brodowski, S., Amelung, W., 2004. Interactive priming of black carbon and glucose mineralization. Org. Geochem. 35, 823–830.

Harris, D., Horwath, W.R., van Kessel, C., 2001. Acid fumigation of soils to remove carbonates prior to total organic carbon or carbon-13 isotopic analysis. Soil Sci. Soc. Am. J. 65, 1853–1856.

IPCC, 2022. Climate Change 2022: Impacts, Adaptation, and Vulnerability. In: Pörtner, H.-O., Roberts, D.C., Tignor, M., Poloczanska, E.S., Mintenbeck, K., Alegría, A., Craig, M., Langsdorf, S., Löschke, S., Möller, V., Okem, A., Rama, B. (Eds.), Contribution of Working Group II to the Sixth Assessment Report of the Intergovernmental Panel on Climate Change. Cambridge University Press, Cambridge, UK, p. 3056.

Kuzyakov, Y., Bogomolova, I., Glaser, B., 2014. Biochar stability in soil: decomposition during eight years and transformation as assessed by compound-specific ^{14}C analysis. Soil Biol. Biochem. 70, 229–236.

Laird, D.A., 2008. The charcoal vision: a win–win–win scenario for simultaneously producing bioenergy, permanently sequestering carbon, while improving soil and water quality. Agron. J. 100, 178–181.

Lehmann, J., Joseph, S., 2015. Biochar for Environmental Management - Science and Technology, second ed. Earthscan, London.

Liu, S., Zhang, Y., Zong, Y., Hu, Z., Wu, S., Zhou, J., Jin, Y., Zou, J., 2016. Response of soil carbon dioxide fluxes, soil organic carbon and microbial biomass carbon to biochar amendment: a meta-analysis. Glob. Change Biol. Bioenergy 8, 392–406.

Lopez-Capel, E., Sohi, S.P., Gaunt, J.L., Manning, D.A.C., 2005. Use of thermogravimetry-differential scanning calorimetry to characterize modelable soil organic matter fractions. Soil Sci. Soc. Am. J. 69, 136–140.

Lorenz, K., Lal, R., 2014. Biochar application to soil for climate change mitigation by soil organic carbon sequestration. J. Plant Nutr. Soil Sci. 177, 651–670.

Lugato, E., Lavallee, J.M., Haddix, M., Panagos, P., Cotrufo, M.F., 2021. Different climate sensitivity of particulate and mineral-associated soil organic matter. Nat. Geosci. 14, 295–300.

Mathews, J.A., 2008. Carbon-negative biofuels. Energy Pol. 36, 940–945.

Moreno, J.L., Bastida, F., Díaz-López, M., Li, Y., Zhou, Y., López-Mondéjar, R., Benavente-Ferraces, I., Rojas, R., Rey, A., García-Gil, J.C., Plaza, C., 2022. Response of soil chemical properties, enzyme activities and microbial communities to biochar application and climate change in a Mediterranean agroecosystem. Geoderma 407, 115536.

Morrison, W.E., Pringle, A., van Diepen, T.A.L., Grandy, A.S., Melillo, J.M., Frey, S.D., 2019. Warming alters fungal communities and litter chemistry with implications for soil carbon stocks. Soil Biol. Biochem. 132, 120–130.

Osipov, V.Y., Baranov, A.V., Ermakov, V.A., Makarova, T.L., Chungong, L.F., Shames, A. I., Takai, K., Enoki, T., Kaburagi, Y., Endo, M., Vul', A.Y., 2011. Raman characterization and UV optical absorption studies of surface plasmon resonance in multishell nanographite. Diam. Relat. Mater. 20, 205–209.

Perkins-Kirkpatrick, S.E., Gibson, P.B., 2017. Changes in regional heatwave characteristics as a function of increasing global temperature. Sci. Rep. 7, 12256.

Plante, A.F., José, M., Fernández, J.M., Leifeld, J., 2009. Application of thermal analysis techniques in soil science. Geoderma 153, 1–10.

Plaza, C., Giannetta, B., Fernández, J.M., López-de-Sá, E.G., Polo, A., Gascó, G., Méndez, A., Zaccone, C., 2016. Response of different soil organic matter pools to biochar and organic fertilizers. Agric. Ecosyst. Environ. 225, 150–159.

Plaza, C., Gascó, G., Méndez, A., Zaccone, C., Maestre, F.T., 2018. Chapter 2. Soil organic matter in dryland ecosystems. In: García, C., Nannipieri, P., Hernández, T. (Eds.), The Future of Soil Carbon: its Conservation and Formation. Elsevier, pp. 39–70.

Poll, C., Marhan, S., Back, F., Niklaus, P.A., Kandeler, E., 2013. Field-scale of soil temperature and precipitation change soil CO_2 flux in a temperate agricultural ecosystem. Agric. Ecosyst. Environ. 165, 88–97.

R Core Team, 2021. R: A Language and Environment for Statistical Computing. R Foundation for Statistical Computing, Vienna. https://www.R-project.org.

Ravel, B., Newville, M., 2005. ATHENA, artemis, hephaestus: data analysis for X-ray absorption spectroscopy using IFEFFIT. J. Synchrotron Radiat. 12, 537–541.

Rocci, K.S., Lavallee, J.M., Stewart, E., C, E., Cotrufo, M.F., 2021. Soil organic carbon response to global environmental change depends on its distribution between mineral-associated and particulate organic matter: a meta-analysis. Sci. Total Environ. 793, 1459–148569.

Rovira, P., Vallejo, V.R., 2000. Examination of thermal and acid hydrolysis procedures in characterization of soil organic matter. Commun. Soil Sci. Plant Anal. 31, 81–100.

Samaniego, L., Thober, S., Kumar, R., Wanders, N., Rakovec, O., Pan, M., Zink, M., Sheffield, J., Wood, E.F., Marx, A., 2018. Anthropogenic warming exacerbates European soil moisture droughts. Nat. Clim. Change 8, 421–426.

Sarauer, J.L., Page-Dumroese, D.S., Coleman, M.D., 2019. Soil greenhouse gas, carbon content, and tree growth response to biochar amendment in western United States forests. Glob. Change Biol. Bioenergy 11, 660–671.

Sardans, J., Peñuelas, J., Estiarte, M., 2008. Changes in soil enzymes related to C and N cycle and in soil C and N content under prolonged warming and drought in a Mediterranean shrubland. Appl. Soil Ecol. 39, 223–235.

Schnitzer, M., Hoffman, I., 1966. A thermogravimetric approach to the classification of organic soils. Soil Sci. Soc. Am. Proc. 30, 63–66.

Sohi, S.P., Krull, E., Lopez-Capel, E., Bol, R., 2010. A review of biochar and its use and function in soil. Adv. Agron. 105, 47–82.

Tramblay, Y., Koutroulis, A., Samaniego, L., Vicente-Serrano, S.D., Volaire, F., Boone, A., Le Page, M., Llasat, M.C., Albergel, C., Burak, S., Cailleret, M., Kalin, K.C., Davi, H., Dupuy, J.-L., Greve, P., Grillakis, M., Hanich, L., Jarlan, L., Martin-StPaul, N., Martínez-Vilalta, J., Mouillot, F., Pulido-Velazquez, D., Quintana-Seguí, P., Renard, D., Turco, M., Türkeş, M., Trigo, R., Jean-Philippe Vidal, J.-F., Vilagrosa, A., Zribi, M., Polcher, J., 2020. Challenges for drought assessment in the Mediterranean region under future climate scenarios. Earth Sci. Rev. 210, 103348.

Wang, J., Xiong, Z., Kuzyakov, Y., 2016a. Biochar stability in soil: meta-analysis of decomposition and priming effects. Glob. Change Biol. Bioenergy 8, 512–523.

Wang, Y., Gao, S., Li, C., Zhang, J., Wang, L., 2016b. Effects of temperature on soil organic carbon fractions contents, aggregate stability and structural characteristics of humic substances in a Mollisol. J. Soils Sediments 16, 1849–1857.

Woolf, D., Amonette, J.E., Street-Perrott, F.A., Lehmann, J., Joseph, S., 2010. Sustainable biochar to mitigate global climate change. Nat. Commun. 1, 56.

Yousaf, B., Liu, G., Wang, R., Abbas, Q., Imtiaz, M., Liu, R., 2017. Investigating the biochar effects on C-mineralization and sequestration of carbon in soil compared with conventional amendments using the stable isotope ($\delta^{13}C$) approach. Glob. Change Biol. Bioenergy 9, 1085–1099.

Yu, Z., Ling, L., Singh, B.P., Luo, Y., Xu, J., 2020. Gain in carbon: deciphering the abiotic and biotic mechanisms of biochar-induced negative priming effects in contrasting soils. Sci. Total Environ. 746, 141057.

Zimmerman, A.R., Gao, B., Ahn, M.-Y., 2011. Positive and negative carbon mineralization priming effects among a variety of biochar-amended soils. Soil Biol. Biochem. 43, 1169–1179.